Land Surface Temperature Mapping and Analysis of Moss Banks in the Western Antarctic Peninsula using a multi-sensor UAV

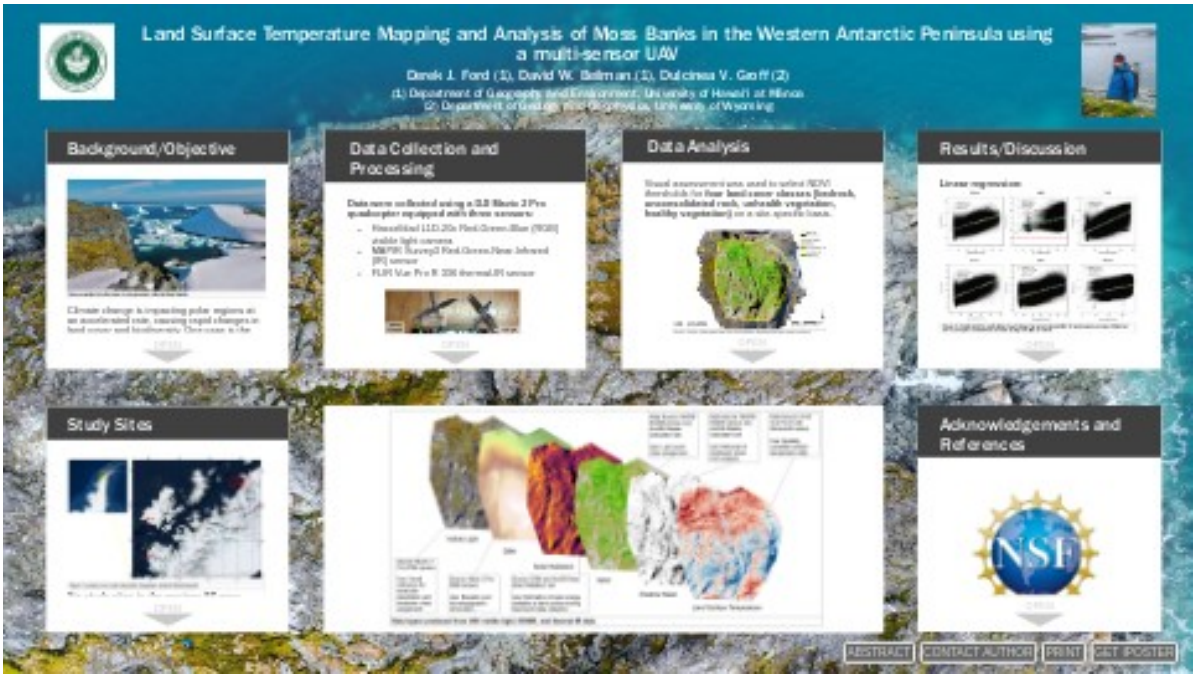

Derek J. Ford (1), David W. Beilman (1), Dulcinea V. Groff (2)

(1) Department of Geography and Environment, University of Hawai'i at Mānoa
(2) Department of Geology and Geophysics, University of Wyoming

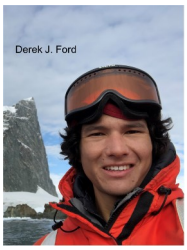

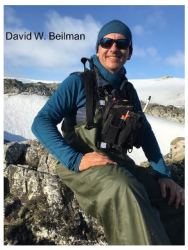

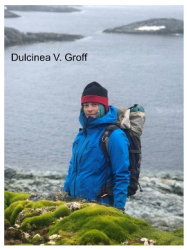

PRESENTED AT:

BACKGROUND/OBJECTIVE

Snow-covered and ice-free areas in close proximity at the Berthelot Islands.

Climate change is impacting polar regions at an accelerated rate, causing rapid changes in land cover and biodiversity. One case is the **"greening up" of the western Antarctic Peninsula (AP)** (Amesbury et al. 2017), the result of:

- Receding glacial fronts (Cook et al. 2005) exposing substrate for plants and soil development.
- Higher temperatures and potential increases in cloud-free conditions conducive to plant growth (Longton 1988; Perera-Castro et al. 2020)

The 2019/2020 austral summer was the warmest on record for the western AP (Robinson et al. 2020), yet the **controls on land surface temperature (LST) here are not well understood.**

Unmanned aerial vehicle (UAV) technology has become an important tool for very-high resolution remote sensing. Rapid development of miniaturized sensors now allows for low-cost multispectral data collection from UAV platforms, and concurrent development of data processing techniques are allowing for more meaningful data interpretation. Previous studies have successfully utilized UAV for studying Antarctic moss banks (Malenovsky et al. 2017; Turner et al. 2018).

Here we present a novel application of multi-sensor UAV data collection and analysis for very high-resolution vegetation, LST, and solar radiation mapping across multiple moss banks in the western AP.

DATA COLLECTION AND PROCESSING

Data were collected using a DJI Mavic 2 Pro quadcopter equipped with three sensors:

- Hasselblad L1D-20c Red-Green-Blue (RGB) visible light camera
- MAPIR Survey3 Red-Green-Near-Infrared (IR) sensor
- FLIR Vue Pro R 336 thermal-IR sensor

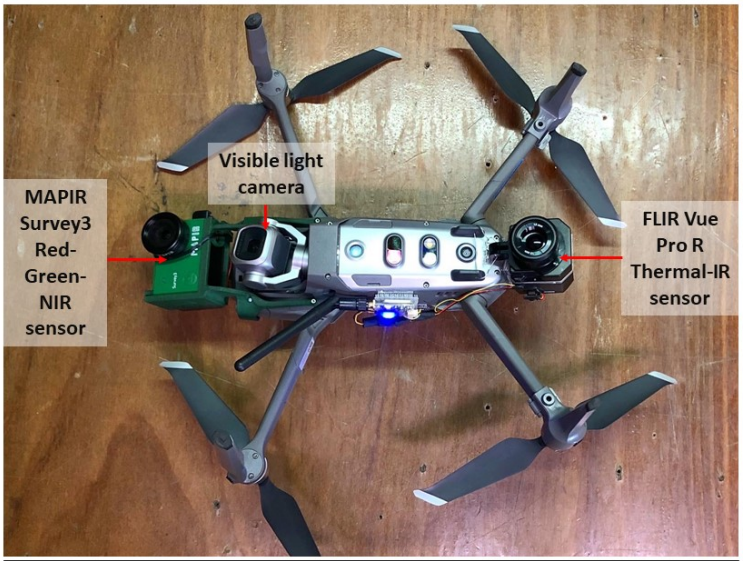

Figure 5. DJI Mavic 2 Pro UAV with two additional sensors attached (bottom view).

Figure 6. DJI Mavic 2 Pro UAV with two additional sensors attached (top view).

Figure 7. DJI Mavic 2 Pro UAV with two additional sensors attached (corner view).

UAV autonomous mapping flights were planned and implemented using flight planning app DroneDeploy. Two monitors were used during UAV operations: a remote controller-mounted iPhone which provided live video, and a secondary monitor for live thermal-IR video, to confirm thermal-IR sensor functioning.

Figure 8. Remote control and thermal-IR video monitor for use in UAV data collection.

Data collection details for the six sites:

- Collection dates - February 22 to March 16, 2020.
- Collection times - Varied from 12:00 to 18:00 local time (GMT+3).
- Collection duration - Less than one hour at each site.
- Atmospheric conditions - Clear and sunny for four sites (MS2, TUX, CHA, CCV), and full overcast with imminent snow at two sites (APE, NOR).

Control points were used for co-registration of the different data layers. At each study site, eight to 12 black-and-white 30×30cm control point flags were distributed, and their locations recorded using a handheld Garmin GPSMap 66 . Aluminum discs were attached to the control points to improve visibility by the thermal-IR sensor.

Figure 9. Control point used for co-registration of the three sensor datasets. Aluminum disc placed in middle of control point increases detectability in thermal-IR data.

Data processing was accomplished with Agisoft Metashape Pro. For each study site, **four data products were exported in TIFF format** at their highest resolution:

- RGB visible light orthomosaic (2cm)
- Digital surface model (DSM) (2cm)
- RGNIR orthomosaic (1cm)
- Thermal-IR orthomosaic (4cm)

Surface solar radiation (WH/m-2) was calculated using the Area Solar Radiation tool in ArcGIS Pro, which was supplied with the UAV-derived DSM and the date/time of data collection. Solar radiation was calculated for the hour immediately before UAV data collection.

Normalized difference vegetation index (NDVI) was calculated for each study site, using the red and near-IR bands from the MAPIR Survey3 sensor. A shadow mask was also derived from these two bands, as the average of red and near-IR. **Shadowed areas were masked out of the analysis**, because they contained large amounts of noise in the near-IR band. Areas with snow were masked out manually, as there were only a few small patches within the study sites.

LST (ºC) was calculated from each thermal-IR orthomosaic using the manufacturer-provided conversion equation.

DATA ANALYSIS

Visual assessment was used to select NDVI thresholds for **four land cover classes (bedrock, unconsolidated rock, unhealth vegetation, healthy vegetation)** on a site-specific basis.

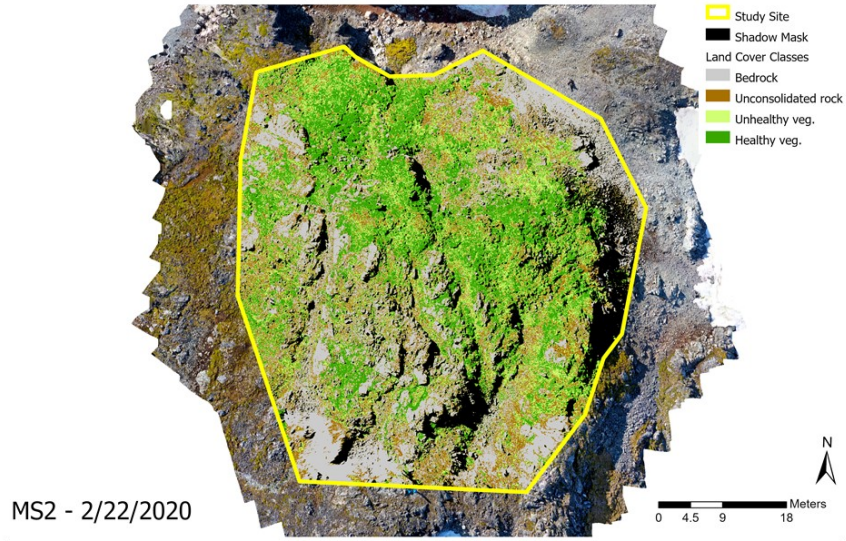

Figure 11. Example of NDVI-guided land cover class assignment. Shadowed areas were masked out and not considered in this study.

Linear regression was used to study the **relationship between LST and solar radiation** for each land cover class at each study site.

Two sets of LST data were used in this analysis. Firstly LST derived from the thermal-IR orthomosaic was used, which covered the full extent of each study site. Secondly, LST derived from individual thermal-IR images, or orthophotos, which covered 73% to 89% of each study site, was also considered. It was decided to do this comparison due to the potential for data blending and noise introduction during thermal-IR orthomosaic production.

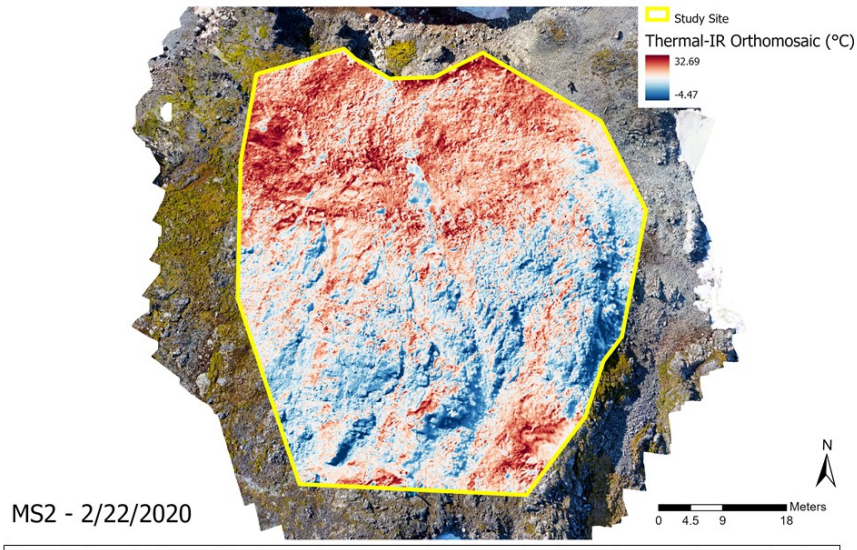

Figure 12. Example of thermal-IR orthomosaic produced by Agisoft Metashape Pro photogrammetric processing of thermal-IR images.

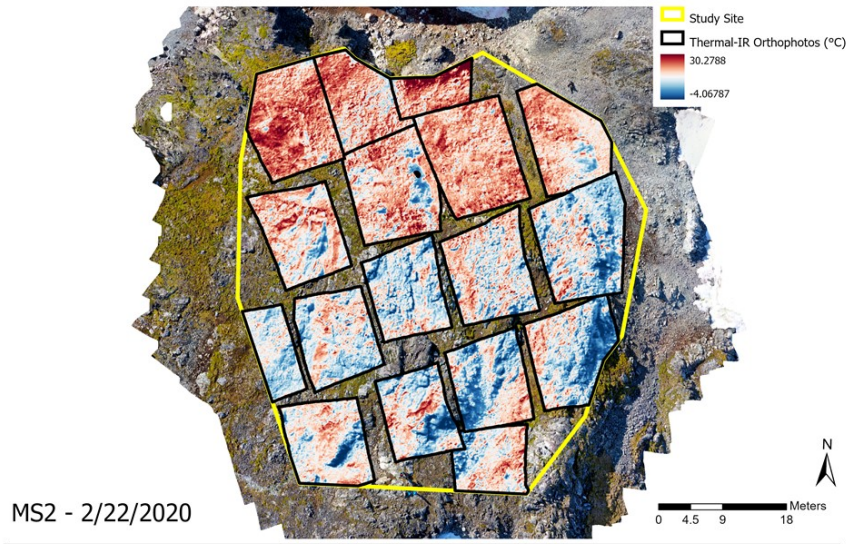

Figure 13. Example of thermal-IR orthophotos covering approximately 76% of the study site.

RESULTS/DISCUSSION

Linear regression:

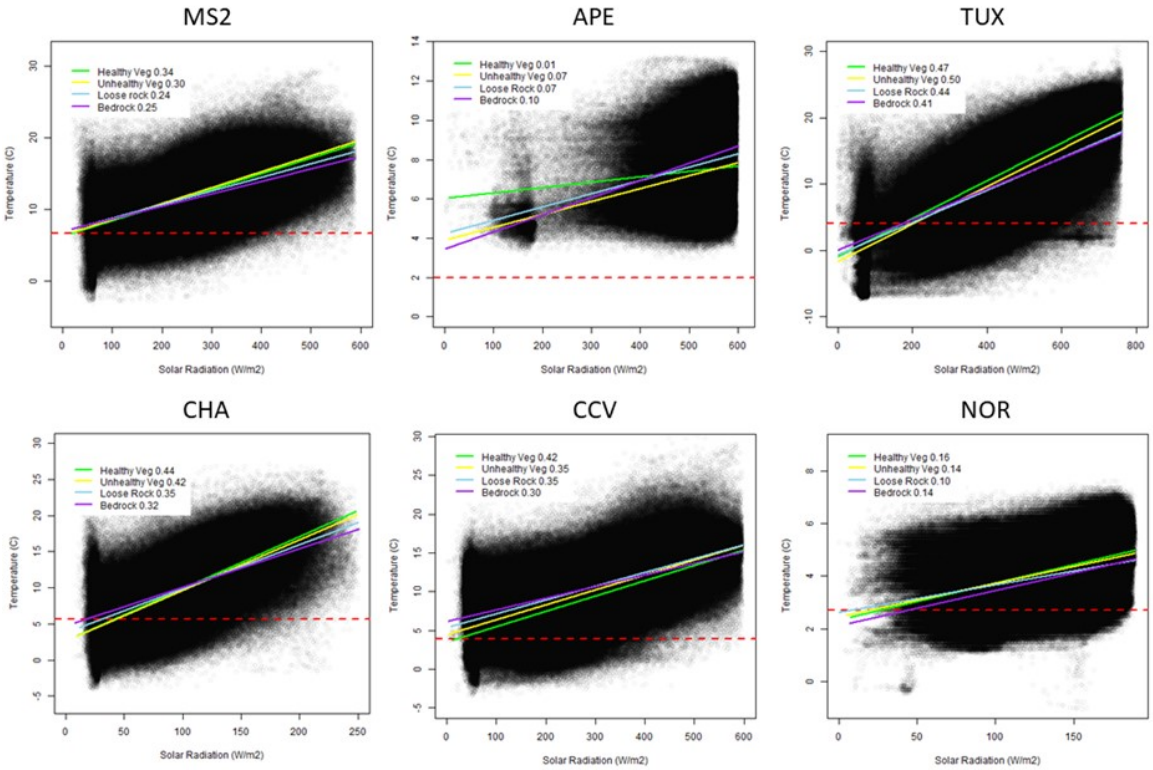

Figure 14. Scatterplots for each study site with linear regression line and R-2 for each landcover class. Dotted red line is average air temperature recorded during UAV data collection.

Average overall R-2 of 0.28 was calculated for all landcover classes and study sites. Among the four land cover classes, **vegetation showed a stronger relationship between LST and solar radiation than non-vegetation**, with healthy vegetation gaining the highest average R-2, and bedrock gaining the lowest average R-2. Highest maximum R-2 of 0.50 was gained by the unhealthy vegetation class at study site TUX.

Table 1. Study site information and R-2 values. Values presented here are from linear regression using OP-derived LST.

						R-2					p-value
Study Site	date	start time	end time	Air temp (C)	PAR	Overall (all classes)	Bedrock	Loose rock	Unhealthy veg	Healthy veg	Overall (all classes)
MS2	2/22/2020	16:28	16:50	6.6	2226	0.27	0.25	0.24	0.30	0.34	P<0.001
APE	2/23/2020	12:28	13:18	2	885	0.06	0.10	0.07	0.07	0.01	P<0.001
TUX	3/3/2020	13:11	13:39	4.1	1686	0.46	0.41	0.44	0.50	0.47	P<0.001
CHA	3/7/2020	17:16	18:01	5.7	1649	0.40	0.32	0.35	0.42	0.44	P<0.001
CCV	3/8/2020	15:11	15:59	3.9	1143	0.35	0.30	0.35	0.35	0.42	P<0.001
NOR	3/16/2020	11:55	12:00	2.7	166	0.13	0.14	0.10	0.14	0.16	P<0.001
			Average:			0.28	0.25	0.26	0.29	0.31	

Comparison of thermal-IR orthomosaic and thermal-IR orthophotos:

It was found that linear regression performed using LST derived from the **thermal-IR orthophotos resulted in higher R2 than LST derived from the thermal-IR orthomosaic**. The two sites with highest photosynthetically active radiation (PAR) (MS2 and TUX) showed the greatest difference of up to 15% between the LST data sources.

Table 2. Comparison of results using LST derived from the thermal-IR orthomosaic (OM) or from the thermal-IR orthophotos (OP).

	Orthomosaic (OM)					Orthophotos (OP)				
Study Site	**Overall**	**Healthy Veg**	**Unhealthy Veg**	**Loose Rock**	**Bedrock**	**Overall**	**Healthy Veg**	**Unhealthy Veg**	**Loose Rock**	**Bedrock**
MS2	0.15	0.13	0.14	0.18	0.19	0.27	0.25	0.24	0.30	0.34
APE	0.06	0.09	0.08	0.07	0.02	0.06	0.10	0.07	0.07	0.01
TUX	0.37	0.35	0.38	0.40	0.35	0.46	0.41	0.44	0.50	0.47
CHA	0.38	0.32	0.31	0.39	0.43	0.40	0.32	0.35	0.42	0.44
CCV	0.39	0.36	0.40	0.39	0.45	0.35	0.30	0.35	0.35	0.42
NOR	0.12	0.15	0.11	0.15	0.11	0.13	0.14	0.10	0.14	0.16
Average	0.24	0.23	0.24	0.26	0.26	0.28	0.25	0.26	0.29	0.31
Overall difference (OP - OM) (%)	3.4%	1.9%	2.2%	3.3%	4.9%					

Discussion:

Vegetation shows a stronger relationship between solar radiation and surface temperature than non-vegetation. The continued greening of Antarctica may exhibit a **positive feedback of further increasing land surface temperatures with increasing vegetation coverage**. Very recent study shows that Antarctic mosses achieve optimal growth at higher temperatures (above 20°C) (Perera-Castro et al. 2020), re-enforcing this positive feedback effect.

Data from the **thermal-IR orthophotos were more informative than those from the thermal-IR orthomosaic**. This is likely due to information lost during the orthomosaic production process. Nevertheless, the same trends were detected in both datasets showing that thermal-IR orthomosaic production is a useful approach.

Simultaneous UAV-based data collection proved to be useful for the purpose of this study. All data sources could be successfully processed and co-registered through use of control points visible within all imagery.

Further research will explore the use of UAV imagery as reference data for satellite-based NDVI vegetation mapping of Antarctic moss banks.

STUDY SITES

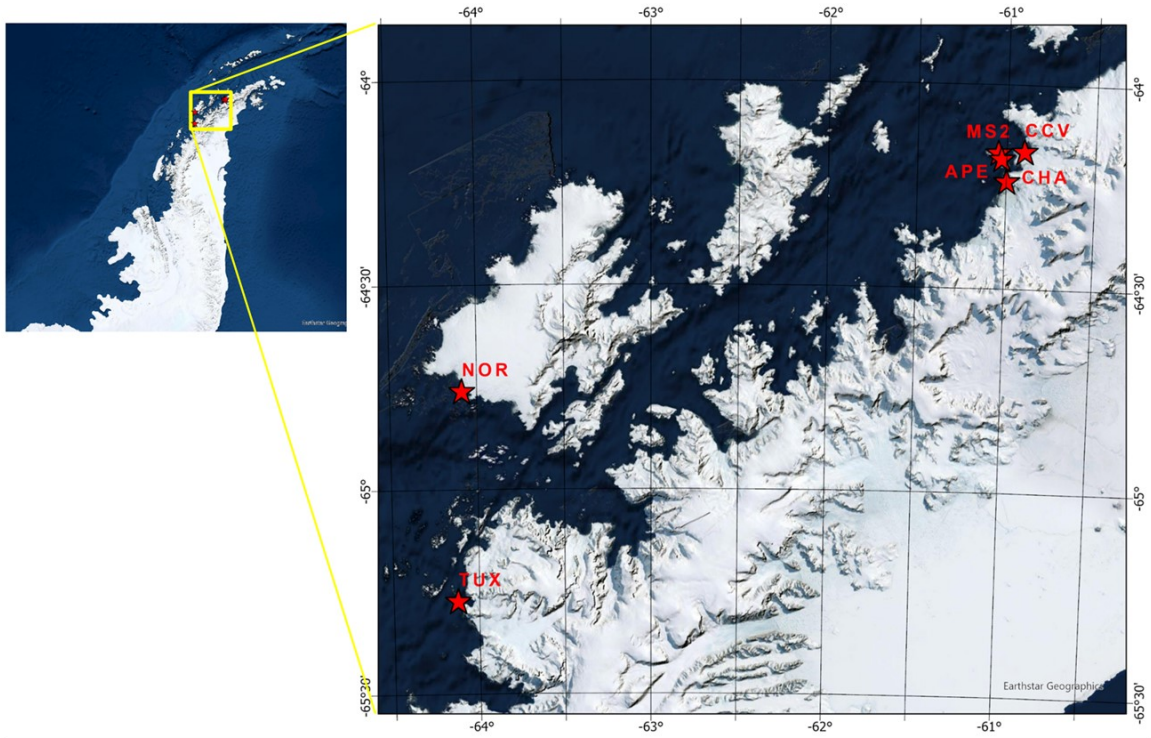

Figure 1. Location of six study sites within the western Antarctic Peninsula (AP).

Six study sites in the western AP were selected for data collection:

- Latitude ranging from 64.16°S to 65.27°S.
- Coastal ice-free areas, ranged in elevation from 3m to 100m MSL.
- 1450m-2 to 7000m-2 in size.

Three sites (MS2, APE, NOR) were located on islands, and the other three (CCV, CHA, TUX) were continental peninsula sites.

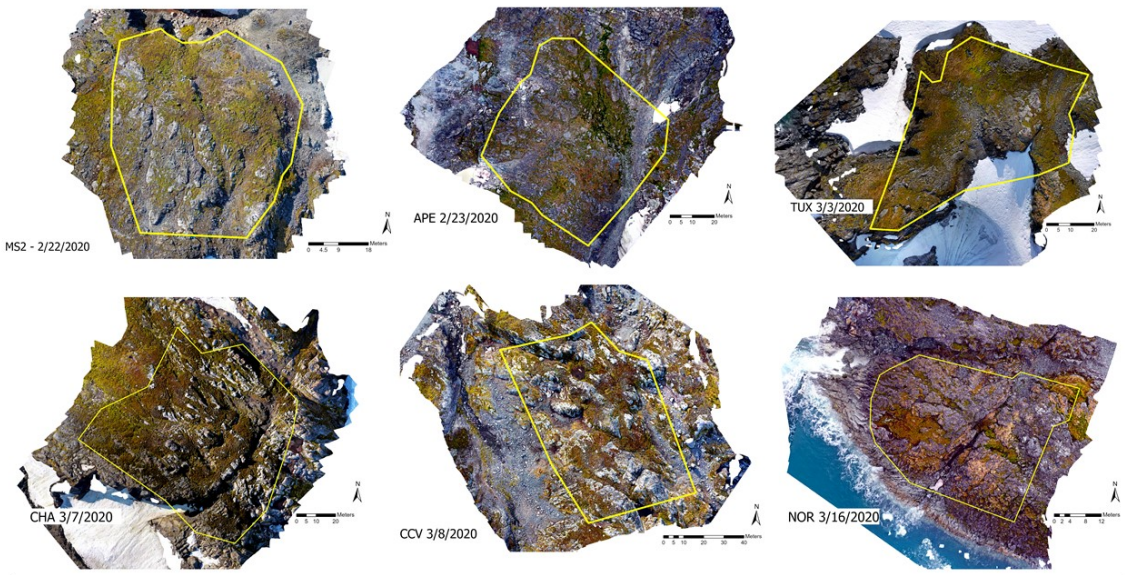

Figure 2. Six study sites with specific study areas outlined in yellow.

These sites were selected for their abundant moss banks primarily composed of one or more dominant peat-forming species,

namely *Polytrichum strictum* and *Chorisodontium aciphyllum*. The sites shared similar characteristics including the presence of many medium to large rock outcroppings along with areas of loose rock and organic matter. All sites were also situated on predominantly north-facing slopes, due to the greater abundance of moss banks oriented in this direction.

Figure 3. Example of an ice-free area with abundant peat-forming moss bank.

Figure 4. Example of an ice-free area with abundant peat-forming moss bank.

[VIDEO] https://www.youtube.com/embed/cxj-Ha_kInY?rel=0&fs=1&modestbranding=1&rel=0&showinfo=0

ACKNOWLEDGEMENTS AND REFERENCES

National Science Foundation:

NSF-1745082 grant to David Beilman, Program Director Mike Jackson

Lehigh University:

Zicheng Yu, Bob Booth

University of Hawaii:

Elizabeth Tajima, Jodi Yamasaki, Hanalei Abbot

US Antarctic Program staff:

Cara Ferrier, Eric Hutt, Nate Williams, Diane Hutt, Adina Scott, Elizabeth Foretek, Amy Schaub, Michael Tepper Rasmussen, Michael Lucibella

Edison Choest Offshore (ship) team:

Zsolt Ezstergomi, George Longshore, Alexander Donovan, Gabriel Garcia, Brian Bell, David Zghaib, Misieli Fineangnofo, Elphren Prado

References:

Amesbury, M. J., Roland, T. P., Royles, J., Hodgson, D. A., Convey, P., Griffiths, H., & Charman, D. J. (2017). Widespread biological response to rapid warming on the Antarctic Peninsula. Current Biology, 27(11), 1616-1622.

Cook, A. J., Fox, A. J., Vaughan, D. G., & Ferrigno, J. G. (2005). Retreating glacier fronts on the Antarctic Peninsula over the past half-century. Science, 308(5721), 541-544.

Longton, R. E. 1988. Adaptations and strategies of polar bryophytes. Bot. J. Linn. Soc 98, 253–268.

Malenovský, Z., Lucieer, A., King, D. H., Turnbull, J. D., & Robinson, S. A. (2017). Unmanned aircraft system advances health mapping of fragile polar vegetation. Methods in Ecology and Evolution, 8(12), 1842-1857.

Perera-Castro, A. V., Waterman, M. J., Turnbull, J. D., Ashcroft, M. B., McKinley, E., Watling, J. R., ... & Robinson, S. A. (2020). It is hot in the sun: Antarctic mosses have high temperature optima for photosynthesis despite cold climate. Frontiers in plant science, 11, 1178.

Robinson, S. A., Klekociuk, A. R., King, D. H., Pizarro Rojas, M., Zúñiga, G. E., & Bergstrom, D. M. (2020). The 2019/2020 summer of Antarctic heatwaves. Global Change Biology.

Turner, D., Lucieer, A., Malenovský, Z., King, D., & Robinson, S. A. (2018). Assessment of Antarctic moss health from multi-sensor UAS imagery with Random Forest Modelling. International journal of applied earth observation and geoinformation, 68, 168-179.

ABSTRACT

Climate change is impacting polar regions at an accelerated rate, causing rapid changes in land cover and biodiversity. One case is the “greening up” of the Western Antarctic Peninsula (WAP), the result of receding glacial fronts exposing substrate for plants and soil development, together with higher temperatures and potential increases in cloud-free conditions conducive to plant growth. The 2019/2020 austral summer was the warmest on record for the WAP, yet the controls on land surface temperature (LST) here are not well understood. We investigated the relationships between land cover type, solar radiation, and LST for several vegetated coastal outcrops (0.3 to 0.5 ha) distributed from 64 to 65°S along the WAP. Remote sensing data was collected in February/March 2020 using a consumer-grade unmanned aerial vehicle (UAV), additionally equipped with near-IR and thermal-IR sensors. Digital surface models produced from the UAV imagery were used to calculate surface solar radiation. NDVI was used to identify four land cover classes: healthy vegetation, unhealthy vegetation, loose substrate, bedrock. Thermal-IR data provided sub-decimeter LST mapping. LST ranges varied depending on atmospheric conditions. A site surveyed under cloud-free conditions and air temperature of 6.6°C showed a 37.2°C range in LST, while a nearby site surveyed the next day under overcast conditions and air temperature of 2°C showed a 10.4°C range in LST. Vegetation at these two sites reached maximum temperatures of 27°C and 11.6°C, respectively. We found little within-site difference in either mean or range of LST among the land cover classes. Using linear regression, solar radiation explained less than 25% of the observed LST. Healthy vegetation showed the strongest relationship between solar radiation and LST. It was determined that LST in the WAP was strongly affected by factors other than solar radiation, implying latent heat effects. As the abundance of healthy vegetation increases in these areas, LST may show a stronger relationship with solar radiation, thus effecting local feedbacks to warming. This study presents the first application of UAV-derived thermal-IR data for the analysis of LST controls in Antarctica, highlighting the capability of UAV as a data collection platform for use in remote and relatively data-poor environments.